

Binding and Internalization in Receptor-Targeted Carriers: The Complex Role of CD44 in the Uptake of Hyaluronic Acid-Based Nanoparticles (siRNA Delivery)

Julio M. Rios de la Rosa, Ponpawee Pingrajai, Maria Pelliccia, Alice Spadea, Enrique Lallana, Arianna Gennari, Ian J. Stratford, Walter Rocchia, Annalisa Tirella,* and Nicola Tirelli*

CD44 is an endocytic hyaluronic acid (HA) receptor, and is overexpressed in many carcinomas. This has encouraged the use of HA to design CD44-targeting carriers. This paper is about dissecting the mechanistic role of CD44. Here, HA-decorated nanoparticles are used to deliver siRNA to both tumoral (AsPC-1, PANC-1, HT-29, HCT-116) and non-tumoral (fibroblasts, differently polarized THP-1 macrophages, HUVEC) human cell lines, evaluating the initial binding of the nanoparticles, their internalization rate, and the silencing efficiency (cyclophilin B (PPIB) gene). Tumoral cells internalize faster and experience higher silencing than non-tumoral cells. This is promising as it suggests that, in a tumor, HA nanocarriers may have limited off-target effects. More far-reaching is the inter-relation between the four parameters of the study: CD44 expression, HA binding on cell surfaces, internalization rate, and silencing efficiency. No correlation is found between binding (an early event) and any of the other parameters, whereas silencing correlates both with speed of the internalization process and CD44 expression. This study confirms on one hand that HA-based carriers can perform a targeted action, but on the other it suggests that this may not be due to a selective binding event, but rather to a later recognition leading to selective internalization.

often, while we may have some mechanistic knowledge of how a delivery vehicle initially binds to such a group, we hardly know what happens during later phases. These phases, however, are equally critical for the efficacy of the treatment: for example, whether a nucleic acid-loaded particle remains on a cell surface or is transported intracellularly can make the difference between therapeutic success and failure. In short, the rational development of a targeted delivery approach should require the understanding of both surface binding and internalization processes, and the interplay between them.


Here, we have focused on these points, using nanoparticles where hyaluronic acid (HA) acts as a targeting element and siRNA is the payload (i.e., the drug). Rather than for cell targeting, HA is better known as a major component of extracellular matrices,^[1] and for its use as a matrix component in regenerative medicine,^[2] as a dermal filler,^[3] or a viscosupplementation agent.^[4]

However, besides its physical properties, HA is also capable of interacting with a number of biomolecules.^[5] Most, but not all HA-binding proteins (also referred to as hyaladherins) share a homologous, HA-binding Link domain, whose

1. Introduction

Identifying an appropriate group (e.g., a cell-surface receptor) is the key step of any targeted delivery-based therapy. Most

Dr. J. M. Rios de la Rosa,^[†] Dr. A. Spadea, Dr. E. Lallana, Dr. A. Tirella
NorthWest Centre for Advanced Drug Delivery (NoWCADD)
School of Health Sciences
University of Manchester
Oxford Road, Manchester M13 9PT, UK
E-mail: annalisa.tirella@manchester.ac.uk

 The ORCID identification number(s) for the author(s) of this article can be found under <https://doi.org/10.1002/adhm.201901182>.

© 2019 The Authors. Published by WILEY-VCH Verlag GmbH & Co. KGaA, Weinheim. This is an open access article under the terms of the Creative Commons Attribution License, which permits use, distribution and reproduction in any medium, provided the original work is properly cited.

^[†]Present address: Cambridge Enterprise Limited, University of Cambridge, Hauser Forum, 3 Charles Babbage Rd, Cambridge CB3 0GT, UK

^[††]Present address: Orchard Therapeutics, 108 Cannon Street, EC4N 6EU London, UK

P. Pingrajai, Dr. M. Pelliccia,^[††] Dr. A. Spadea, Dr. E. Lallana,
Dr. I. J. Stratford, Dr. A. Tirella, Prof. N. Tirelli
Division of Pharmacy and Optometry
Faculty of Biology, Medicine and Health
University of Manchester
Manchester Academic Health Science Centre
Oxford Road, Manchester M13 9PL, UK
E-mail: nicola.tirelli@iit.it

Dr. A. Gennari, Prof. N. Tirelli
Laboratory for Polymers and Biomaterials
Fondazione Istituto Italiano di Tecnologia
16163 Genova, Italy

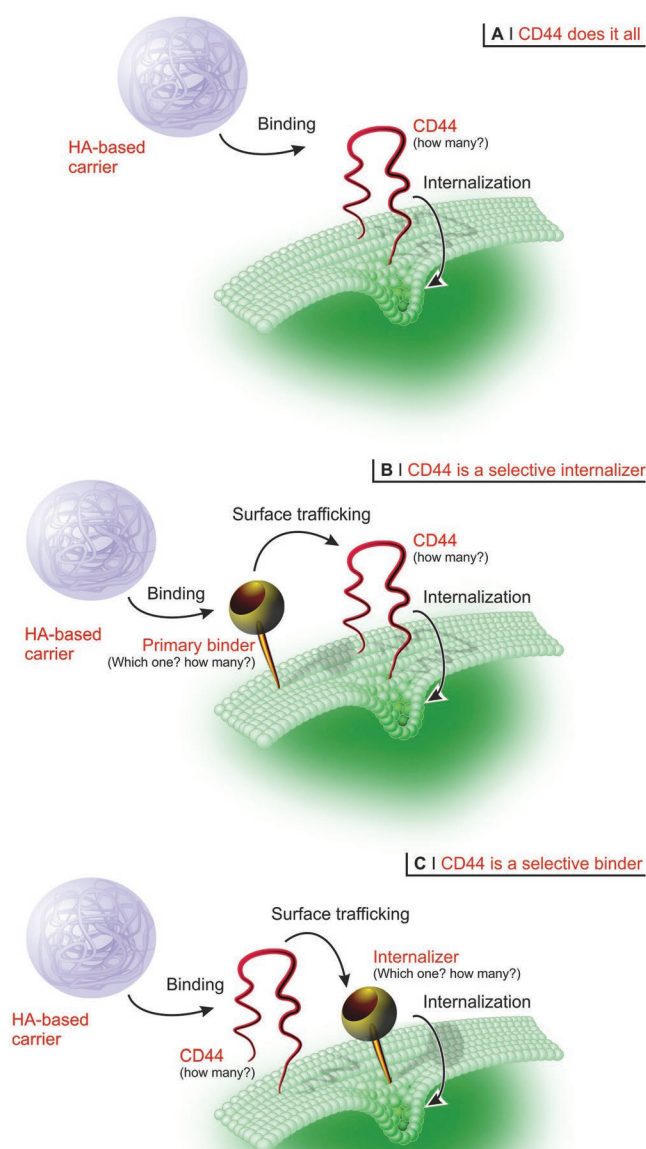
Dr. W. Rocchia
CONCEPT Lab
Fondazione Istituto Italiano di Tecnologia
16163 Genova, Italy

DOI: 10.1002/adhm.201901182

size is critical to determine their affinity toward HA. As recently demonstrated by the group of Richter,^[6] the force necessary to mechanically detach HA increases from type A hyaladherins (short Link domain) such as TSG-6 or Hyaluronic Acid Receptor for Endocytosis (HARE) to type B (medium-length Link) such as CD44, reaching a maximum for type C (long Link) such as aggrecan. Some HA receptors are therapeutically interesting, chiefly CD44 since it is known to be significantly upregulated in cancer-initiating^[7] or metastasizing cells,^[8] with much involvement in the epithelial–mesenchymal transition,^[9] in cancer-(initiating) cell survival,^[10] and drug resistance.^[11] Together with the structurally unrelated Receptor for Hyaluronic Acid Mediated Motility (RHAMM, also known as CD168), CD44 has also important roles in angiogenesis and cell motility.^[12]

Due to such clear association to cancer initiation and poor prognosis, much effort has been devoted to targeting CD44. However, a rational approach to CD44 targeting with HA is complicated by a number of factors, which, as we recently reviewed,^[13] include the following:

- A) CD44 identity. CD44 is present in several isoforms, with a number of post-translational modifications (e.g., deglycosylation,^[14] dimerization,^[15] but also selective cleavage liberating soluble or matrix-bound CD44^[16]) that can affect the affinity for HA. It has been shown indeed that in different cells CD44 can have inactive, inducible, and constitutionally active HA-binding.^[14]
- B) The avidity of the interaction. For example, HA can discriminate between different CD44 densities (“superselective” interaction^[17]), whereas the details of HA exposure on a carrier surface are likely to cause change in the number of CD44 clustered around each carrier,^[18] and through that also the interactions with potential co-receptors.^[19]
- C) The unclear relation between CD44 expression, HA binding and its internalization. Since its discovery, CD44 has been proposed as an endocytic receptor,^[20] and in a recent paper we have shown that there may be a correlation between CD44s (CD44 standard isoform) expression and the internalization rate of soluble HA.^[21] Yet, whether CD44 covers both roles of “binder” and “internalizer,” or mainly only one of them is not known (**Scheme 1**). Using RGD-functionalized (thus integrin-binding) HA, we gathered indication of a more significant role of CD44 in internalization than in initial binding,^[22] and it has been reported that cytoplasmic tail acylation inactivates CD44-mediated HA endocytosis, but not its binding to cells.^[23] However, there are evidences pointing to a link to binding: in differently activated THP-1 macrophages higher CD44 expression (M1>M2,M0) increased HA binding, and slowed down its internalization.^[24]
- D) The possible off-target effects. Although typically overexpressed by malignant cells,^[25] HA in principle can also accumulate at other sites. Accumulation where HA catabolism takes place (i.e., in skin and liver,^[26] either in a CD44^[27] or HARE^[28]-mediated fashion) has a clearly negative effect on therapeutic efficacy, but uptake in nontumoral cells within a tumor microenvironment (TME) may be equally dangerous. This issue is sometimes addressed with an a priori receptor saturation with HA^[29] or chondroitin sulfate, the latter being specifically interesting due to an apparently higher affinity for HARE than for CD44;^[30] another potential strategy is the incorporation of additional and potentially CD44-synergic ligands that can increase cell selectivity.^[19,22,31]



Scheme 1. Sketch of the possible roles of CD44 in the uptake of HA; please note that this is an oversimplification of a likely much more complex situation, above all in the endocytic process. A) CD44 captures HA from the extracellular space (binding) and then orchestrates its internalization in endocytic vesicles. Importantly, the stoichiometry of the interaction (number of HA vs number of CD44) is likely variable, and the degree of CD44 clustering may have profound effects on both intracellular signaling and the mechanism and kinetics of endocytosis. B) One or more different receptors may be responsible for the initial binding, with unknown specificity and selectivity, then transferring HA to CD44 for a more selective interaction and eventually its internalization. C) Alternatively, the additional receptor(s) may preside over the internalization of HA, after the latter has initially bound CD44.

Here, we have used HA-decorated nanoparticles: They comprise chitosan as a cationic component and siRNA when a payload is employed, but HA is the major component and dictates the surface properties and the interactions presiding to

cell uptake.^[18b,32] As cellular models, we have selected a panel of human cell lines that represent the variety of cellular types possibly present in a solid tumor: “real” cancerous cells (two models each for pancreatic and colorectal cancer) and noncancerous cells (variously polarized macrophages, fibroblasts, and endothelial cells), the latter being potentially responsible for off-target effects in cancer therapy. All these cells are also likely characterized by different levels of CD44 expression. In this paper, we then aim to highlight whether a relationship exists between CD44 expression and extent of binding, internalization rate and silencing activity (i.e., the points B to D of the above list). We here also want to acknowledge the main limit of this study: we have assumed (a) all CD44 variants to be equally good in their interactions with HA, and (b) the differential effects of post-translational modifications to be negligible, in comparison to those of the differences in CD44 expression. This means that point A in the above list is not tackled.

2. Experimental Section

We report in Supporting Information, Sections S1 and S2, the following information: general cell culture methods and identity of the immortalized human cell lines used in this study (Section S1.1, Supporting Information), preparation of concentrated cell culture media (Section S1.2, Supporting Information), protocols used for macrophage polarization (Section S1.3, Supporting Information), and the methods used for the analysis of CD44 expression (Section S2, Supporting Information).

Preparative Operations—Labeling of HA with Rhodamine B (HA-Rho): HA ($\overline{M}_w = 180$ kDa) was kindly provided by Kyowa (Milan, Italy) and covalently conjugated to Lissamine rhodamine B ethylenediamine (Thermo Scientific, UK) via 4-(4,6-dimethoxy-1,3,5-triazin-2-yl)-4-methylmorpholinium chloride (DMTMM, Sigma-Aldrich, UK) mediated acylation. Briefly, 100 mg of HA (0.25 mmol of carboxylate units) were dissolved in 10 mL of HEPES buffer 100×10^{-3} M pH = 7.4 under mild stirring overnight. Then, 2 mg of lissamine rhodamine B ethylenediamine dye (0.00325 mmol, targeted degree of carboxylate substitution = 1%, 1.3 eq.) dissolved in 2.5 mL of HEPES buffer were added followed by addition of 2.5 mL of a 65×10^{-3} M solution of DMTMM (0.1625 mmol, 0.65 eq.) in HEPES buffer. The reaction mixture was stirred (300 rpm) for 24 h at 25 °C, then quenched and precipitated by addition of a 20-fold volume excess of cold ethanol 96% (v/v). The resulting dispersion was left overnight at 4 °C to allow complete precipitation of the polymer. The precipitate was isolated by centrifugation (10 min at 4500g), dissolved in 10 mL of deionized water, and purified by dialysis (MWCO = 20 kDa) against deionized water. Finally, the solution containing HA-Rho conjugate was freeze-dried (mass recovery: 70%). The degree of functionalization was calculated by measuring the fluorescence intensity of the fluorescently labeled HA (Ex: 540/25, Em: 620/40 nm; Synergy2 Biotek plate reader equipped with Gen5 software) using Lissamine Rhodamine B Ethylenediamine dye to calculate the emission to the molar concentrations of the fluorophore (please note that this is later transformed in a molar ratio between the dye-functionalized and nonfunctionalized monomer units in the polymer). Typical degree of derivatization: 0.7–1.0% mol of carboxylate units.

Preparative Operations—Preparation and Characterization of Chitosan/HA Nanoparticles: All the materials used for the handling of siRNA were either nuclease-free or sequentially washed with RNaseZap solution (Thermo Scientific, UK), 70% (v/v) ethanol in water, and nuclease-free water (Thermo Scientific, UK) prior to use. Chitosan with average viscosimetric molecular weight (\overline{M}_v) = 656 kDa and degree of deacetylation 85% (middle-viscosity chitosan) was purchased from Sigma-Aldrich, UK. Chitosan with $\overline{M}_v = 36$ kDa was obtained by oxidative degradation of a 1% wt. middle-viscosity chitosan solution in 0.1 M HCl/ 3×10^{-3} M sodium nitrite. Chitosan samples were purified in-house prior to use as previously described.^[19] Nanoparticles were prepared by direct polyelectrolyte complexation of chitosan with siRNA and HA in aqueous medium. This preparative method encompasses first the preparation of a 0.069% wt. chitosan solution. Both low ($\overline{M}_v = 36$ kDa) and high ($\overline{M}_v = 656$ kDa) molecular weight (MW) chitosan were dissolved overnight in 4.6×10^{-3} M HCl (aq), then the pH value was adjusted to 5 by adding 0.1 M NaOH (aq). HA was dissolved overnight in nuclease-free water at a concentration of 1.5 mg mL⁻¹, and the pH value was adjusted to 5 by adding 0.1 M HCl (aq). The siRNA solutions were prepared at the desired concentration by diluting the 100×10^{-6} M stock (stored at -20 °C) with nuclease-free water. The chitosan and HA solutions were filtered through 0.45 and 0.22 μ m pore size filters (Merck Millipore, UK), respectively. For non-siRNA containing nanoparticles, the chitosan solution was further diluted 1:2 (v/v) with sterile nuclease-free water. For the preparation of siRNA-loaded nanoparticles, the siRNA solution (prepared in nuclease-free water, nucleic acid concentration depending on the targeted %wt. loading) was gently pipetted in a same volume of chitosan solution and the initial complexation step was carried in 2.0 mL round-bottom Eppendorf tube under magnetic agitation (1000 rpm) for 10 min at 25 °C. HA-decorated nanoparticles (chitosan/HA) were finally obtained by addition of the chitosan solution or chitosan/siRNA suspension into an equal volume of 1.5 mg mL⁻¹ HA solution under the same stirring conditions allowing the complexation for 30 min at 25 °C.

Dynamic light scattering (DLS) analysis of the hydrodynamic size, ζ -potential, and polydispersity index (PDI) of chitosan/HA nanoparticles was performed on three independent samples (as prepared) at 25 °C using a Zetasizer Nano ZS instrument (Model ZEN3600, Malvern Instruments Ltd., UK) equipped with a solid-state HeNe laser ($\lambda = 633$ nm, scattering angle of 173°). The size and polydispersity data were calculated by using the General-purpose algorithm. The electrophoretic mobility of the samples was converted into ζ -potential by using the Smolouchowski equation.

The encapsulation efficiency (EE) of siRNA in nanoparticles was determined by measuring the amount of noncomplexed nucleic acid remaining in solution. Briefly, chitosan/HA nanoparticles were sedimented via centrifugation (13 000 rpm for 60 min at 4 °C), and the amount of siRNA in solution was quantified via fluorimetry (Synergy2 Biotek plate reader equipped with Gen5 software) using the Quant-iT RiboGreen RNA Assay Kit (Thermo Scientific, UK) as specified by the manufacturer. EE values (%) were calculated as follows: $EE = (A - B)/A \times 100$, where A is the amount of siRNA in the nanoparticle feed, and B is the amount of free siRNA in the supernatant.

Study of Chitosan/HA Nanoparticle–Cell Interactions: Nanoparticle dispersions for cell experiments were prepared in complete cell growth medium at a final working concentration of $125 \mu\text{g mL}^{-1}$ by addition of an equal volume of twofold concentrated complete medium (prepared as described in Section S1.2, Supporting Information) to a twofold concentrated nanoparticle aqueous dispersion (i.e., $250 \mu\text{g mL}^{-1}$). Please note that nanoparticle binding and internalization studies were performed using, respectively, HA-Rho or DY547-labeled siRNA (siGLO Cyclophilin B Control, sequence: 5'-GGA AAG ACU GUU CCA AAAA-3'; No. D-001610-01-05, Dharmacon, UK) as fluorescent reporters. For the avoidance of doubt, these experiments were performed using nanoparticles labeled either at HA or at siRNA, but not with both in order to avoid fluorophore cross-talk issues from interfering with relevant readouts.

Study of Chitosan/HA Nanoparticle–Cell Interactions—Quantification of Nanoparticle Uptake Using Cell Lysates: Cells were plated in Costar polystyrene 12-well plates with flat bottom (No. 3513, Corning, UK) and left adhere overnight (a summary of cell density used is reported in Table S1, Supporting Information). Cells were incubated with $125 \mu\text{g mL}^{-1}$ chitosan/Rho-HA nanoparticles (pH = 6.4) for specific time points (2, 4, 8, 16, and 24 h) in a humidified 5% (v/v) CO_2 air atmosphere at 37°C . Untreated cells were used as a control. After each incubation time, nanoparticle-containing medium was removed, cells were washed three times with phosphate buffered saline (PBS), and finally lysed in $100 \mu\text{L}$ RIPA buffer. The total uptake of HA, comprising both membrane-bound and internalized materials, was estimated from the fluorescence intensity of cell lysates by using a calibration of chitosan/HA-Rho nanoparticles in cell lysates at a concentration range of $0.12\text{--}125 \mu\text{g mL}^{-1}$ using a Synergy2 Biotek plate reader (Ex: 540/25, Em: 620/40 nm) equipped with Gen5 software (sensitivity of the instrument adjusted to wells with the highest nanoparticle concentration of the calibration curve, i.e., $125 \mu\text{g mL}^{-1}$; optical position: top 50%; light source: Xenon flash). The number of cells for each well was estimated by using a standard curve that correlates the number of cells versus protein content for each individual cell line. Finally, the nanoparticle concentration values were normalized against the number of cells per well.

Study of Chitosan/HA Nanoparticle–Cell Interactions—Quantification of Nanoparticle Internalization (Flow Cytometry): Cells were plated in Costar polystyrene 12-well plates with flat bottom (No. 3513, Corning, UK) and left adhere overnight (cell density reported in Table S1, Supporting Information). Cells were incubated with $125 \mu\text{g mL}^{-1}$ chitosan/HA nanoparticles loaded with DY547-labeled siRNA (1.45% wt. with respect to chitosan; pH = 6.4) for specific time points (2, 4, 8, 16, and 24 h) in a humidified 5% (v/v) CO_2 air atmosphere at 37°C . Untreated cells were used as a control. At the end of incubation period, the nanoparticle-containing medium was removed, cells were washed three times with PBS, and detached using Trypsin-EDTA solution (No. 59417C, Sigma-Aldrich, UK) for 10 min at room temperature. Cells were pelleted (1000 rpm, 5 min, 25°C) and resuspended in $400 \mu\text{L}$ PBS. The internalization of DY547-labeled siRNA was determined by flow cytometry on 10 000 live, individual cells with a BD LSR Fortessa cytometer (BD Bioscience, San Jose, CA) equipped with the FACSDiva

software (v8.0.1). Data were analyzed with FlowJo (vX.0.7, Tree Star, Ashland, OR) after gating single and live events in the FSC-A/FSC-H and FSC/SSC windows, respectively. Untreated cells were used as autofluorescence control in order to calculate the median fluorescence intensity (MFI) fold change over time, as well as the percentage of positive events for each cell line/time point tested.

Silencing Experiments: For functional silencing experiments, nanoparticles loaded with siGENOME Cyclophilin B Control siRNA (12.45% wt. with respect to chitosan or A/P (amino/phosphate) ratio = 14) (Sequence: 5'-GGA AAG ACU GUU CCA AAAA-3', No. D-001136-01-20; Dharmacon, UK) were diluted to a final working concentration of $125 \mu\text{g mL}^{-1}$ in complete cell growth medium based on HEPES buffer (pH = 6.4) by the addition of an equal volume of twofold medium to a twofold concentrated nanoparticle aqueous dispersion (i.e., $250 \mu\text{g mL}^{-1}$). Note that these conditions are equivalent to a siRNA concentration of $200 \times 10^{-9} \text{ M}$ per well (or equivalent to $0.67 \mu\text{g}$ of siRNA/well).

Silencing Experiments—Knockdown at the mRNA Level (Real-Time Quantitative Polymerase Chain Reactions (RT-qPCR)): Cells were plated in Costar polystyrene 12-well plates with flat bottom (No. 3513, Corning, UK) and incubated in media based on HEPES buffer at pH = 6.4 containing siRNA-loaded chitosan/HA nanoparticles for 24 h in a humidified 5% (v/v) CO_2 air atmosphere at 37°C . Nanoparticle-containing media were aspirated and cells were lysed with trypsin-EDTA solution after thorough rinsing with PBS. The total RNA was extracted using PureLink RNA mini kits (Applied Biosystems, UK), purified via sequential elution with RNase-free water, and stored at -80°C for long-term use. The total RNA concentration and purity were measured via spectrophotometry (NanoDrop ND-1000; Thermo Fisher Scientific, UK). Samples with a 260/280 nm absorbance ratio in the range 1.80–2.0 were used for reverse transcription using the High Capacity cDNA Reverse Transcription Kits (Applied Biosystems, UK). Reverse transcription was performed using the Peltier Thermal Cycler PTC-200 (MJ Research, Waltham, MA) to yield cDNA for downstream TaqMan gene expression analysis. The TaqMan Gene Expression Master Mix (Life Technologies, UK) was used alongside human cyclophilin B (PPIB) (Hs00168719_m1) and human glyceraldehyde-3-phosphate dehydrogenase (GAPDH) (Hs02758991_g1), the latter utilized as an endogenous control. The real-time polymerase chain reactions were carried out in MicroAmp Fast Optical 96-Well Reaction Plates (Applied Biosciences, UK) on a StepOnePlus (Life Technologies, UK) equipped with StepOne software. All reactions were carried out for a total of 40 thermal cycles. Results were run against the house-keeping gene (GAPDH) in a $\Delta\Delta\text{CT}$ quantitative evaluation method and all results were expressed as fold change in gene expression relative to negative control samples (i.e., cells not exposed to siRNA against Cyclophilin B). All qPCR experiments were run on $n = 3$ different wells (technical replicates) and each experiment was repeated three times (biological replicates).

Statistical Analysis: Statistical analyses were performed with GraphPad Prism 8.2 (GraphPad Software, Inc., San Diego, CA). Differences between groups (one-way ANOVA analysis in Figure 2B and *t*-test analysis in Figure 5A) were considered significant at a *P*-value of <0.05 . No preprocessing of raw data

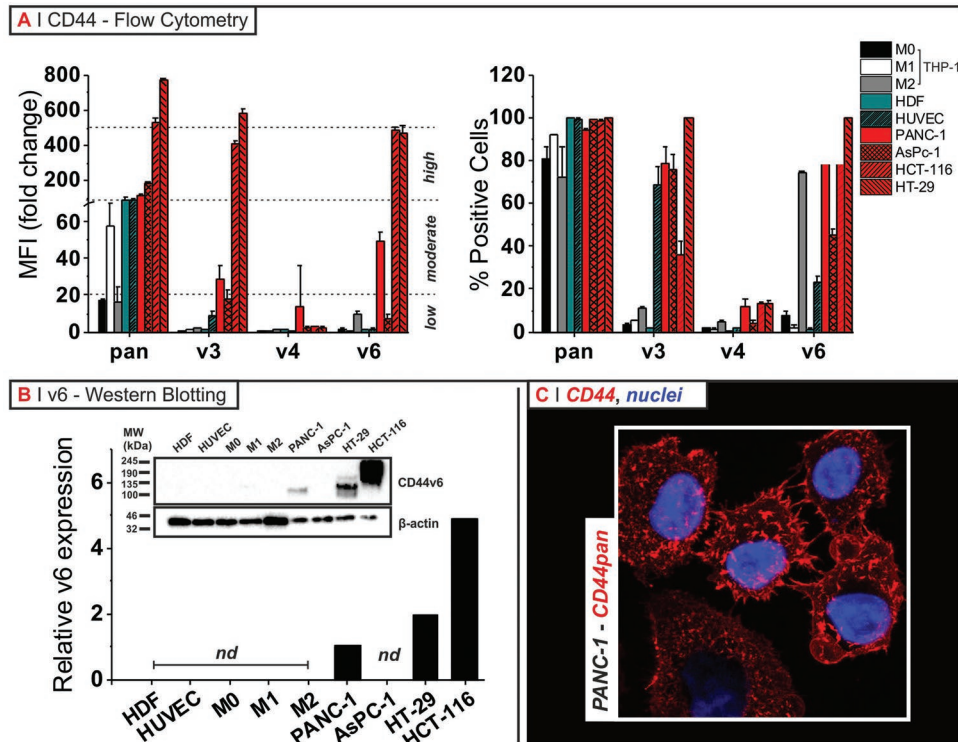


Figure 1. CD44 expression in cancer (colorectal and pancreatic cell lines) and normal (fibroblasts, macrophages, and endothelial cells) cell lines. A) Expression of total CD44 (CD44pan) and CD44 variants (CD44v3, CD44v4, and CD44v6) measured by flow cytometry after indirect staining with AlexaFluor647-labeled antibody. Histogram of *n*-fold change in median fluorescence intensity (MFI) relative to the intensity of the isotype control (left), and percentage of positive cells for the various cell populations (right) are expressed as average \pm SD ($n = 3$). B) Example of Western blot analysis of CD44v6 detected using anti-CD44v6 (2F10) under reducing conditions; when cells were positive to v6, in different cells this variant associated to different molecular weights (≈ 100 kDa for PANC-1, ≈ 140 kDa for HT-29, ≈ 140 – 245 kDa for HCT-116) that likely reflect rather different CD44 isoforms. Since the antibody may bind differently to them, this comparison should be taken as purely qualitative also due to the faint character of the bands for most cells), and only to corroborate flow cytometry data. β -actin was used as loading control; nd = nondetected (columns present the averages for $n = 2$). C) Volume rendering of PANC-1 confocal microscopy, showing nuclei (blue) and the distribution of CD44pan (red) (experimental protocol: see the Experimental Section).

(e.g., transformation, removal of outliers) was performed before statistical analysis, except in the case of silencing efficiency (%) shown in Figure 5 which are a result of the normalization of protein expression levels of each formulation against the protein expression levels of untreated control samples. Data of experimental replicates are presented as mean \pm SD.

In Figure 5D, the correlation analysis was based on averages and standard deviations ($n = 9$ for silencing, $n = 3$ for all other measurements), which were used, under the assumption of Gaussian distribution, to calculate the linear correlation coefficients, and the corresponding SD, relating the observed properties, namely, amount of CD44 expression, extent of binding, internalization rate, and silencing efficiency, over a set of 1000 randomly generated samples.

3. Results and Discussion

3.1. CD44 Expression in Cellular Models

We have characterized CD44 expression in a panel of human cell lines composed of pancreatic (AsPC-1 and PANC-1) and colorectal (HCT-116 and HT-29) cancer cells, and of “off-target”

TME controls, that is, fibroblasts (HDF), endothelial cells (HUVEC), and differently polarized macrophages (THP-1). It is noteworthy that AsPC-1^[33] and HCT-116^[34] are specifically accepted as metastatic models.

We have analyzed the total expression of CD44 (CD44pan: standard and all variants) and that of its most common variant isoforms (CD44v3, CD44v4, and CD44v6) using flow cytometry (Figure 1A) and Western blotting. The latter technique, however, showed strong limitations in the quantification of CD44 expression, despite employing the same primary antibodies. This could be possibly due to differential binding in the likely partially denaturing conditions used in Western blotting: For example, a strictly quantitative comparison of CD44pan expression through the panel was not possible, and the results showed a very significant discrepancy with flow cytometry (in particular for HCT-166 and HT-29; see Section S2.4 and Figure S1, Supporting Information). Another factor may be a poor CD44pan detection in cells with high variant expression. Additionally, Western blotting against variant exons v3 and v4 did not reveal any bands for any of the cell lines (data not shown), while flow cytometry allowed for a full analysis of these two variants. Therefore, we have used flow cytometry for quantitation and Western blotting for a merely qualitative confirmation.

The highest CD44pan expression was detected in colorectal cancer cell lines (Figure 1A, left), well known to express CD44 in large amounts.^[35] Also pancreatic tumoral cell lines,^[36] fibroblasts,^[37] and endothelial cells^[38] are known to produce high levels of CD44, and here they showed comparable CD44pan levels, although lower than the colorectal HCT-116 and HT-29. Macrophages, on the contrary, produced low level of the protein; confirming our previous results,^[39] higher levels are expressed by the M1 subtype, and indistinguishable (lower) amounts by the M0 and M2 subtypes.

CD44 isoforms containing variant exons v3 (CD44v3) and v6 (CD44v6) were detected in all cancer models, albeit in lower amounts in AsPC-1 and PANC-1,^[36b] while were absent in most off-target cells, with the exception of M2 macrophages (these potentially tumor-associated subtype express low, but significant levels of CD44v6^[39]) and HUVEC, which are positive for CD44v3.^[40] Isoforms containing exon v4 (CD44v4) were absent in virtually all cell types, with a marginal expression of a small population (less than 20%) of PANC-1 cells.^[41]

Qualitatively, Western blotting confirmed these findings (see Sections S2.3 and S2.5, and Figure S1, Supporting Information): predominant expression of the CD44 standard isoform (CD44s; CD44pan bands at 85–90 kDa) in HDF,^[42] HUVEC,^[43] and THP-1,^[36a,39] and that of high MW isoforms (CD44pan bands at 140–200 kDa) for HT-29 and HCT-116, with essentially the same order in CD44v6 expression (HCT-116 \gg HT-29 > PANC-1; compare Figure 1B with Figure 1A left). Of note, the prevalent expression of CD44s in AsPC-1 and PANC-1, with small amounts of variants, is also confirmed by higher molecular weight/low intensity bands at longer exposure times (see Figure S1, Supporting Information). Last, as typically seen, CD44 has always a cell surface localization (Figure 1C).

3.2. Preparation and Physicochemical Properties of HA-Decorated Nanoparticles

As a model of HA-displaying nanocarriers, we have used chitosan/HA nanoparticles (Figure 2A); they were prepared by a

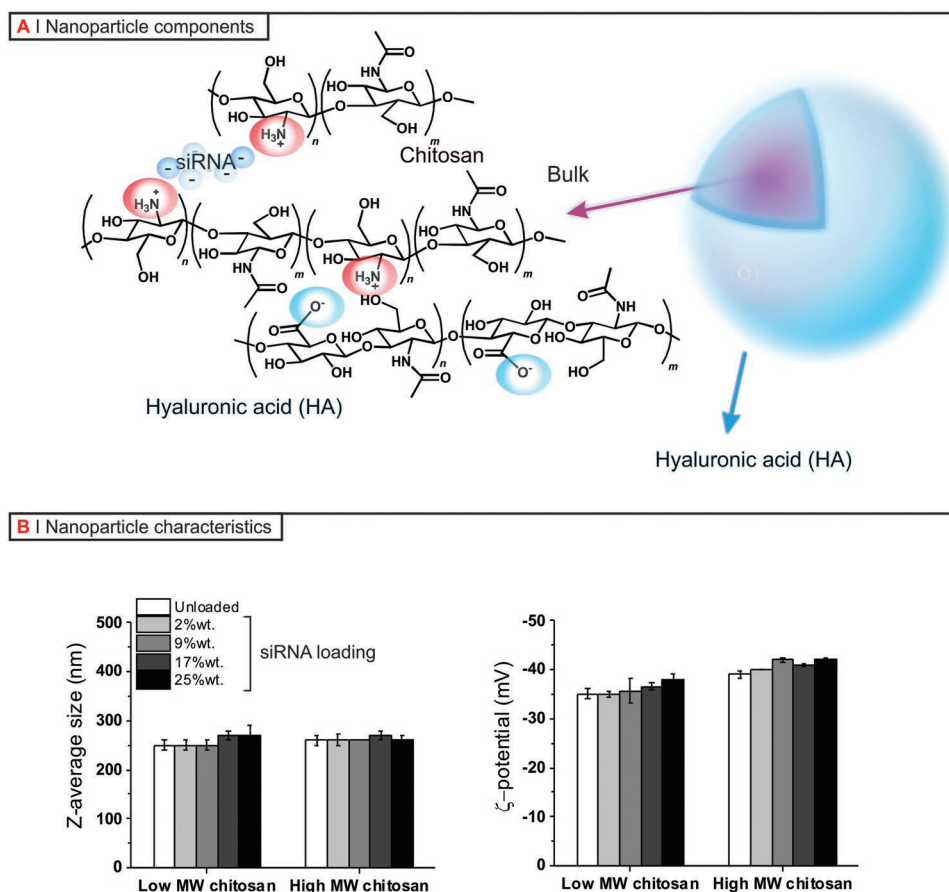


Figure 2. A) Schematic representation of siRNA-loaded chitosan/HA nanoparticles (blue: negative charges; orange: positive charges). Due to the two-step preparative procedure, the bulk is supposed to be predominantly composed of the anionic nucleic acid cargo complexed with the positively charged chitosan (their combination providing a purple color in the sketch), with some degree of penetration of the anionic HA, which however is progressively enriched by approaching the surface; the latter can be assumed to be solely composed of HA. B) Hydrodynamic size (left) and zeta potential (right) of chitosan/HA nanoparticles as a function of siRNA loading. All data are represented as the average \pm SD ($n = 3$). Statistical analysis returned no significant differences (P -values > 0.05) for either size or surface charge between particles prepared from the same chitosan MW but loaded with different amounts of siRNA (one-way ANOVA).

two-stage polyelectrolyte complexation, where chitosan was precomplexed with siRNA and then HA. We have employed chitosan with two very different MW to produce nanoparticles with a different binding strength between the polycationic (chitosan) component and HA, which typically influences the silencing efficiency;^[32b] please refer to our previous paper for a detailed study of the stability of the particles and of the complexation strength (avidity) of chitosan toward RNAs.^[32b] Of note, similar nanoparticles prepared through a triphosphate (TPP)/chitosan intermediate complexation presented HA to murine cells in a fashion that depended on chitosan MW;^[18b,19,32a] the different preparative method employed here ensures that the nanoparticles have the same HA presentation (subject of a forthcoming publication) and therefore differ primarily in their internal cohesion. Both low and high MW chitosan/HA nanoparticles had an average hydrodynamic size of ≈ 250 nm up to high siRNA loading (EE always $>99\%$); since HA is used in excess, it composes the nanoparticle surface, as demonstrated in the negative zeta potential (Figure 2B, right). The main descriptors of the particles were not affected by the amount of siRNA up to 25% wt. in relation to chitosan, hence we conclude that within this limit the level of siRNA loading has no significant influence on at least the initial nanoparticle interactions with cells, that is, in the process of their uptake.

It is worth mentioning here that previous studies of ours demonstrate that the uptake of these nanoparticles is dependent on CD44/HA, since it can be strongly reduced either with HA pretreatment or with CD44-blocking antibodies in HCT-116^[32b] or THP-1 macrophages.^[24]

3.3. Nanoparticle Cell Surface Binding and Internalization Kinetics

We used nanoparticles featuring HA-Rho and a DY547-labeled siRNA cargo, and measured the fluorescence of the former to monitor nanoparticle uptake in cell lysates, and that of the second to follow their internalization via flow cytometry on trypsinized cells. As recently demonstrated,^[39] since trypsin degrades CD44 and thus detaches any CD44-bound material from cell surfaces,^[44] this method allows to selectively follow the nanoparticle internalization kinetics, whereas cell lysates encompass both internalized and surface bound materials.

From cell lysates, it is apparent that nanoparticle uptake reached a plateau already by 2 h incubation for all cellular models (Figure 3A), which indicates a rapid binding and saturation of HA receptor(s). On the other hand, internalization proceeds at a much slower pace (Figure 3B), reaching plateau values after 16–24 h of incubation, with virtually complete transfection of all cell populations (see Figure S2, Supporting Information, left).

Two numerical parameters can be extracted, which allow to quantitate the two phases of nanoparticle uptake:

A) The binding, that is, the amount of nanoparticles bound “per cell.” This was obtained by converting the cell lysate fluorescence at 4 h into the actual concentration of nanoparticles, and then normalizing the latter against the protein content; notably, flow cytometry measurements at 4 h show not only low amounts of internalized particles but also very low numbers of positive cells (see Figure S2, Supporting Information,

right), indicating that at this point cell lysate fluorescence is almost solely reflective of binding.

B) The internalization rate. This is obtained directly as the flow cytometry signal read at 24 h. Please note that this parameter may slightly underestimate the rate for HCT-116, since they appear to be already at plateau after 16 h.

Rather surprisingly, binding showed very little, if any, dependency on the total CD44 expression (Figure 4A); all cells showed similar binding for the two kinds of particles, which indicates an HA presentation independent of chitosan MW; note that we previously demonstrated such a dependency, but only on murine cells.^[18b,19,32a] As visually depicted in Figure 4A through the use of dashed lines, the only apparent relationship is the separation of macrophages—as low binders with low CD44 content—from all other cells that can generically be seen as high binders. Within the macrophage subtypes, we confirm our previous results that M1 produce more CD44 and are better binders than M0 and M2.

On the other hand, the nanoparticle internalization rate scaled reasonably with CD44pan (Figure 4B); it is possible to see a reasonable alignment in a log-log plot (green line in Figure 4B), with the exception of HT-29 (CD44^{high}, but slow in internalization) and M1 macrophages. Two explanations of this behavior that we are inclined to discount are that: (A) HT-29 express highly an isoform (CD44v6) known to associate into protein complexes, e.g., with c-Met and HGF,^[45] which can possibly reduce its endocytic performance (in favor of a signaling role); this should have been observed also for HCT-116. (B) Slower nanoparticle internalization in M1 than M0 and M2 may be due to their more aggressive endocytic conditions, leading to fluorophore degradation: this should have been seen also in cell lysate analysis. However, when comparing relatively similar cells, that is, M1 versus M0 and M2 (all macrophages) and HT-29 versus HCT-116 (colon carcinomas with epithelial origin), it is noticeable that a higher CD44 level corresponds to a poorer internalization; this may suggest that—within the constraints of similar cells—the density of CD44 may have optimal values for internalization above which the process is slowed down.

An important conclusion of this phase of the study is that HA-decorated nanoparticles are more rapidly internalized in tumoral rather than in “healthy” (although possibly tumor-associated) cell types, which is encouraging from the perspective of the minimization of off-target effects.

3.4. Therapeutic Performance (Silencing)

In this part of the study, we have used the cyclophilin B (PPIB) gene as a silencing target: Not only PPIB has an abundant and comparable expression across most cell lines (healthy and cancerous) but also more importantly it is a nonessential gene and its knockdown does not compromise cell viability.^[46] The siRNA concentration used in transfection experiments (200×10^{-9} M, obtained with a 12.45% wt. loading in $125 \mu\text{g mL}^{-1}$ nanoparticles) was optimized in preliminary experiments performed on HCT-116 using Lipofectamine LTX as a transfection agent (see Section S4 and Figure S3, Supporting Information). We recently demonstrated that silencing capabilities of such nanoparticles were comparable to Lipofectamine LTX, and that

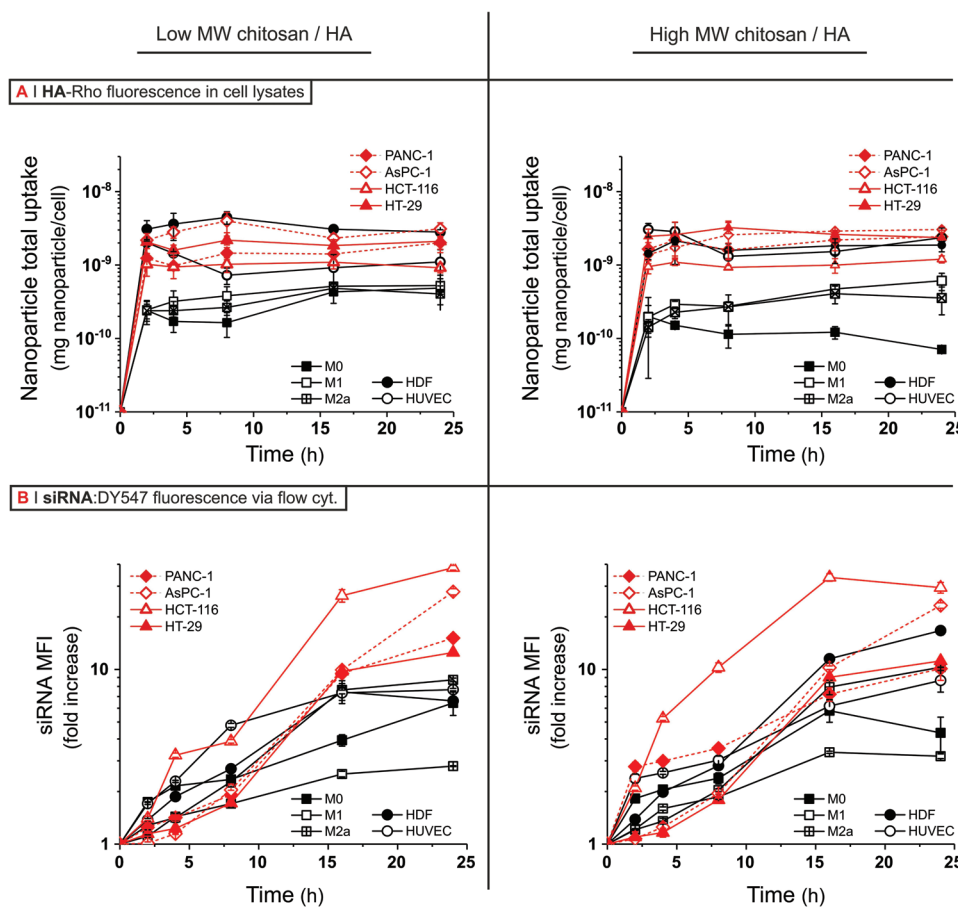


Figure 3. A) Nanoparticle uptake, that is, binding and internalization, of low (left) and high (right) MW chitosan/HA nanoparticles ($125 \mu\text{g mL}^{-1}$) obtained by measuring HA-Rho fluorescence in cell lysates as a function of time and normalizing it against the cell number (please note that each cell type has its own calibration curve protein content vs cell number). B) Internalization kinetics of the same nanoparticles measured by monitoring the fluorescence of the nanoparticle siRNA cargo (1.45% wt. in relation to chitosan—loading optimized for fluorescence detection) by flow cytometry on live cells. The MFI-fold (relative to untreated control) is directly proportional to the nanoparticle internalization of intact particles and does not include material bound to the cell membrane due to trypsin treatment. All data are represented as the average \pm SD ($n = 3$).

nanoparticles maintained such capability even after storage or exposure to nucleases.^[47]

Markedly different silencing values were obtained in the different cell models (Figure 5A), ranging from hardly any effect on M1 macrophages, to low (and variable) silencing in M0/M2 macrophages, HUVEC, and HDF, and also HT-29 ($\approx 30\text{--}40\%$ PPIB mRNA reduction), to increasingly higher outcomes in AsPC-1 and PANC-1 ($\approx 50\text{--}60\%$ reduction) and in HCT-116 cells ($\approx 70\text{--}80\%$ reduction). A first conclusion is, therefore, to confirm that HA nanoparticles are promising for the minimization of potential off-target effects. Of note, no significant differences could be ascribed to the chitosan MW.

When pooling together all silencing data (all cell types, two types of nanoparticles; Figure 5B; see also Section S5 and Figure S4, Supporting Information), it is apparent that no clear correlation exists with the nanoparticle binding on the cell surface (cell lysates at 4 h). On the contrary, PPIB silencing appears to have much a clearer relation with internalization rate and also with CD44 expression (Figure 5C). We have then utilized the linear correlation coefficient, ranging from -1 (perfect

anticorrelation), to 0 (no correlation), to 1 (perfect positive correlation), to quantify the interrelations between the four variables investigated in this study, that is, CD44 expression, binding extent, internalization rate, and silencing efficiency (Figure 5D). The final result is, as expected from the data presented in Figures 4B and 5C, that a statistically significant correlation exists between silencing efficiency and internalization, and to a lesser extent also between silencing and CD44 availability.

The first correlation is easy to explain: An efficient gene silencing requires an efficient internalization of the siRNA carriers. The comparatively homogeneous nanoparticle behavior, however, may also suggest that they all had a similar mechanism of endosomal escape. The second correlation is somehow surprising, because at the same time neither correlates with the extent of cell binding but also possibly more revealing: This behavior is consistent with HA being rapidly bound by low specificity (e.g., scavenging) receptors, and only later trafficked to CD44 as a more selective binder and internalizer. It goes without saying that this is only one of the possible interpretations of the experimental results. However, the

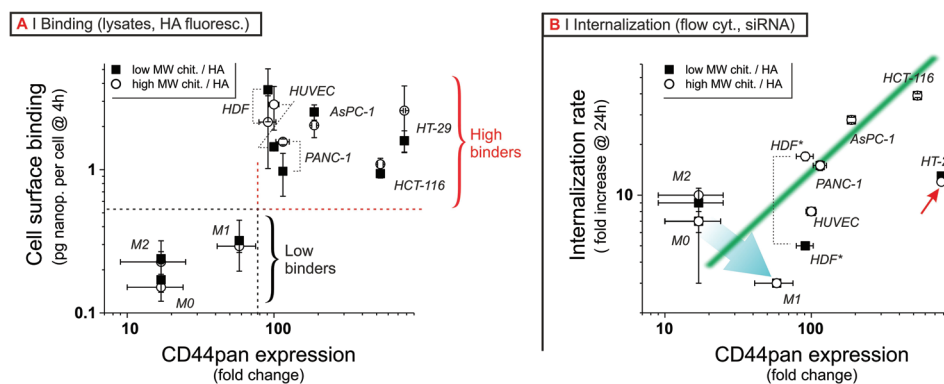


Figure 4. Correlation (log–log plots) between the expression of total membrane-bound CD44 (CD44pan; measured through indirect staining flow cytometry) and A) nanoparticle uptake/binding (HA-Rho, cell lysate at 4 h), B) siRNA median fluorescence intensity (MFI) fold change/internalization (DY547-labeled siRNA, flow cytometry at 24 h) of low and high MW chitosan/HA nanoparticles (left and right column graphs, respectively). Data are represented as the average \pm SD ($n = 3$). Please note that the dotted red/black and the solid green lines are just guides for the eyes.

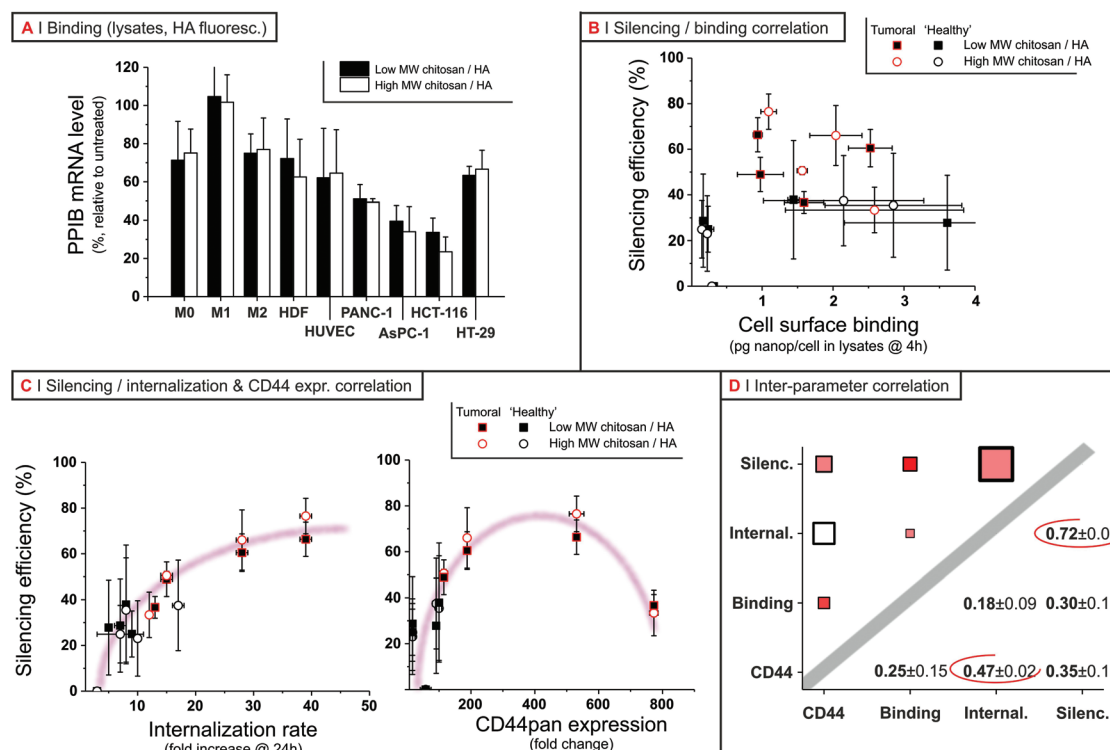


Figure 5. A) Knockdown of PPIB transcription (measured by RT-qPCR) upon 24 h treatment with low and high MW chitosan/HA nanoparticles loaded with anti-PPIB siRNA (12.45% wt. with respect to chitosan, corresponding to an A/P (amine/phosphate) ratio of 14 and to a siRNA concentration of 200×10^{-3} M). Please note that all experiments were performed at pH 6.4 to mimic the tumor's interstitial pH, and also to rule out any effect of nanoparticle stability seen at higher pH. The silencing was evaluated after the 24 h incubation, immediately after nanoparticle removal. Experimental data are expressed as average \pm SD ($n = 9$, three biological replicates, with three technical replicates each). Statistical analysis returned no significant differences (P -values > 0.05) in PPIB mRNA silencing efficiency between the two chitosan MW for each cell line (t -test, two-tailed). B) Correlation between PPIB silencing efficiency (as described in (A)) and cell binding as calculated from the lysate fluorescence at 4 h normalized against the protein content. C) Correlation between silencing efficiency and internalization rate (left; amount of internalized siRNA at 24 h, MFI-fold over untreated control) and CD44 pan expression (right; MFI-fold expression over isotype). The purple curves are just guides for the eyes. The relatively low silencing in HT-29 may have the same cause of their relatively slow nanoparticle internalization. D) Cross-correlation between the main parameters describing the therapeutic efficiency of CD44-mediated cell targeting. Due to the properties of the correlation matrix, that is, symmetry and self-correlation equal to 1, only the nontrivial entries are shown. The bottom right half of the graph provides the numerical values of the correlation coefficient. The upper left half of the graph expresses these data with more visually through symbols with a size proportional to the value of the correlation coefficient and a color coding of their precision (red for the highest standard deviation, white for the lowest).

hypothesized mechanism, if confirmed, would have profound implications for the very definition of targeting: In fact, the HA-mediated targeting of CD44 should not be interpreted as a cell surface event of selective binding, but rather as a more complex phenomenon of endocytic recognition.

4. Conclusion

This study can provide two interesting conclusions. The first, more directly relevant to drug delivery, is that—within the limits of a relatively small panel of cell lines—tumoral cells appear to be more easily and efficiently targeted and treated by HA-decorated nanoparticles. This finding is specifically relevant when considering that a very significant portion of virtually any tumoral mass is composed by nontumoral cells, and generally there is no direct therapeutic advantage in their treatment. The *caveat* inherent to this picture is that, on the basis of expression profile of CD44pan or of its more tumor-associated variants, colorectal cell lines would seem a priori the most suitable models to evaluate CD44-targeting cancer therapies. However, HT-29 cells—both CD44^{high} and CD44^{v^{high}}—contradict this simplistic prediction; the take-home message is therefore that CD44 expression cannot be employed as the only predictive element for an HA-based therapy.

The second concept is very relevant to the concept of “targeted delivery.” HA/CD44 interactions appear capable of conferring selectivity to internalization processes; however, different cell surface binding events probably occur before them, and may not be selective. Therefore, while the therapeutic outcome (PPIB silencing) has a significant statistical correlation with CD44 expression and thus it may be possible to call it a targeted action, its efficacy may be reduced by nonselective binding (which does not imply treatment) on nontarget cells. Admittedly, our experimental basis has a relatively small size, but hopefully we have shed some light onto the probably general concept that a targeted intracellular delivery may actually happen in the absence of a highly specific binding event.

Supporting Information

Supporting Information is available from the Wiley Online Library or from the author.

Acknowledgements

J.M.R.d.I.R. is indebted to EPSRC for a Ph.D. studentship as part of the North-West Nanoscience (NoWNano) Doctoral Training Centre (EPSRC Grant No. EP/G03737X/1). The Bioimaging Facility and Flow Cytometry Facility (FBMH, University of Manchester) are maintained with grants from BBSRC, Wellcome Trust, and the University of Manchester Strategic Funds. A.T. was partially funded through the Innovate UK project number 101710. M.P. and A.G. gratefully acknowledge financial support from the EU FP7 project UniVax (Grant No. 601738). Kyowa (Milan, Italy) is gratefully acknowledged for the provision of hyaluronic acid. This work was supported by AstraZeneca through the establishment of the NorthWest Centre for Advanced Drug Delivery (NoWCADD) at the University of Manchester.

Conflict of Interest

The authors declare no conflict of interest.

Keywords

cancer, CD44, hyaluronic acid, internalization, nanocarriers, RNA, silencing, targeted drug delivery

Received: August 26, 2019

Revised: October 16, 2019

Published online:

- [1] R. K. Sironen, M. Tammi, R. Tammi, P. K. Auvinen, M. Anttila, V. M. Kosma, *Exp. Cell Res.* **2011**, *317*, 383.
- [2] X. Xu, A. K. Jha, D. A. Harrington, M. C. Farach-Carson, X. Q. Jia, *Soft Matter* **2012**, *8*, 3280.
- [3] K. L. Beasley, M. A. Weiss, R. A. Weiss, *Facial Plast. Surg.* **2009**, *25*, 086.
- [4] A. W. S. Rutjes, P. Juni, B. R. da Costa, S. Trelle, E. Nuesch, S. Reichenbach, *Ann. Intern. Med.* **2012**, *157*, 180.
- [5] A. J. Day, G. D. Prestwich, *J. Biol. Chem.* **2002**, *277*, 4585.
- [6] a) F. Bano, M. I. Tammi, D. W. Kang, E. N. Harris, R. P. Richter, *Biophys. J.* **2018**, *114*, 2910; b) F. Bano, S. Banerji, M. Howarth, D. G. Jackson, R. P. Richter, *Sci. Rep.* **2016**, *6*, 34176.
- [7] S. Zhang, C. Balch, M. W. Chan, H. C. Lai, D. Matei, J. M. Schilder, P. S. Yan, T. H. M. Huang, K. P. Nephew, *Cancer Res.* **2008**, *68*, 4311.
- [8] V. Orian-Rousseau, *Eur. J. Cancer* **2010**, *46*, 1271.
- [9] H. X. Xu, Y. J. Tian, X. Yuan, H. Wu, Q. Liu, R. G. Pestell, K. M. Wu, *OncoTargets Ther.* **2015**, *8*, 3783.
- [10] T. Chanmee, P. Ontong, K. Kimata, N. Itano, *Front. Oncol.* **2015**, *5*, 180.
- [11] Y. Gao, R. Foster, X. Q. Yang, Y. Feng, J. K. Shen, H. J. Mankin, F. J. Hornicek, M. M. Amiji, Z. F. Duan, *Oncotarget* **2015**, *6*, 9313.
- [12] M. Slevin, J. Krupinski, J. Gaffney, S. Matou, D. West, H. Delisser, R. C. Savani, S. Kumar, *Matrix Biol.* **2007**, *26*, 58.
- [13] J. M. R. de la Rosa, A. Tirella, N. Tirelli, *Adv. Biosystems* **2018**, *2*, 1800049.
- [14] N. M. English, J. F. Lesley, R. Hyman, *Cancer Res.* **1998**, *58*, 3736.
- [15] D. C. Liu, M. S. Sy, *J. Immunol.* **1997**, *159*, 2702.
- [16] J. Cichy, E. Pure, *J. Cell Biol.* **2003**, *161*, 839.
- [17] G. V. Dubacheva, T. Curk, R. Auzely-Velty, D. Frenkel, R. P. Richter, *Proc. Natl. Acad. Sci. USA* **2015**, *112*, 5579.
- [18] a) A. Almalik, P. J. Day, N. Tirelli, *Macromol. Biosci.* **2013**, *13*, 1671; b) A. Almalik, S. Karimi, S. Ouasti, R. Donno, C. Wandrey, P. J. Day, N. Tirelli, *Biomaterials* **2013**, *34*, 5369.
- [19] A. Gennari, M. Pelliccia, R. Donno, I. Kimber, N. Tirelli, *Adv. Healthcare Mater.* **2016**, *5*, 966.
- [20] a) M. Culty, H. A. Nguyen, C. B. Underhill, *J. Cell Biol.* **1992**, *116*, 1055; b) Q. Hua, C. B. Knudson, W. Knudson, *J. Cell Sci.* **1993**, *106*, 365.
- [21] A. Spadea, J. M. R. de la Rosa, A. Tirella, M. B. Ashford, K. J. Williams, I. J. Stratford, N. Tirelli, M. Mehibel, *Mol. Pharm.* **2019**, *16*, 2481.
- [22] S. Ouasti, P. J. Kingham, G. Terenghi, N. Tirelli, *Biomaterials* **2012**, *33*, 1120.
- [23] S. P. Thankamony, W. Knudson, *J. Biol. Chem.* **2006**, *281*, 34601.
- [24] J. M. R. de la Rosa, A. Tirella, A. Gennari, I. J. Stratford, N. Tirelli, *Adv. Healthcare Mater.* **2017**, *6*.

- [25] a) S. Hiscox, B. Baruha, C. Smith, R. Bellerby, L. Goddard, N. Jordan, Z. Poghosyan, R. I. Nicholson, P. Barrett-Lee, J. Gee, *BMC Cancer* **2012**, *12*, 458; b) H. J. Wei, T. Yin, Z. Zhu, P. F. Shi, Y. Tian, C. Y. Wang, *Hepatobiliary Pancreatic Dis. Int.* **2011**, *10*, 428; c) D. Naor, S. B. Wallach-Dayana, M. A. Zahalka, R. V. Sionov, *Semin. Cancer Biol.* **2008**, *18*, 260; d) N. M. Resnick, M. R. Clarke, J. M. Siegfried, R. Landreneau, D. C. Asman, L. S. Ge, L. S. Kierstead, G. D. Dougherty, D. L. Cooper, *Mol. Diagn.* **1998**, *3*, 93.
- [26] L. Jadin, L. H. Bookbinder, G. I. Frost, *Matrix Biol.* **2012**, *31*, 81.
- [27] H. Harada, M. Takahashi, *J. Biol. Chem.* **2007**, *282*, 5597.
- [28] B. Zhou, J. A. Weigel, L. A. Fauss, P. H. Weigel, *J. Biol. Chem.* **2000**, *275*, 37733.
- [29] F. A. Venning, L. Wullkopf, J. T. Erler, *Front. Oncol.* **2015**, *5*, 224.
- [30] Y. Luo, M. R. Ziebell, G. D. Prestwich, *Biomacromolecules* **2000**, *1*, 208.
- [31] S. P. Qiao, Y. F. Zhao, S. Geng, Y. Li, X. L. Hou, Y. Liu, F. H. Lin, L. F. Yao, W. M. Tian, *Int. J. Nanomed.* **2016**, *11*, 6667.
- [32] a) A. Almalik, R. Donno, C. J. Cadman, F. Cellesi, P. J. Day, N. Tirelli, *J. Controlled Release* **2013**, *172*, 1142; b) E. Lallana, J. M. R. de la Rosa, A. Tirella, M. Pelliccia, A. Gennari, I. J. Stratford, S. Puri, M. Ashford, N. Tirelli, *Mol. Pharm.* **2017**, *14*, 2422.
- [33] Z. H. Li, K. Chen, P. Jiang, X. Zhang, X. W. Li, Z. H. Li, *Diagn. Pathol.* **2014**, *9*.
- [34] I. L. Botchkina, R. A. Rowehl, D. E. Rivadeneira, M. S. Karpeh Jr., H. Crawford, A. Dufour, J. Ju, Y. Wang, Y. Leyfman, G. I. Botchkina, *Cancer Genomics Proteomics* **2009**, *6*, 19.
- [35] a) T. Ishimoto, O. Nagano, T. Yae, M. Tamada, T. Motohara, H. Oshima, M. Oshima, T. Ikeda, R. Asaba, H. Yagi, T. Masuko, T. Shimizu, T. Ishikawa, K. Kai, E. Takahashi, Y. Imamura, Y. Baba, M. Ohmura, M. Suematsu, H. Baba, H. Saya, *Cancer Cell* **2011**, *19*, 387; b) P. Zhang, C. L. Fu, H. Y. Bai, E. Q. Song, Y. Song, *FEBS Lett.* **2014**, *588*, 4573.
- [36] a) F. Birzele, E. Voss, A. Nopora, K. Honold, F. Heil, S. Lohmann, H. Verheul, C. Le Tourneau, J. P. Delord, C. van Herpen, D. Mahalingam, A. L. Coveler, V. Meresse, S. Weigand, V. Runza, M. Cannarile, *Clin. Cancer Res.* **2015**, *21*, 2753; b) S. Zhao, C. Chen, K. Chang, A. Karnad, J. Jagirdar, A. P. Kumar, J. W. Freeman, *Clin. Cancer Res.* **2016**, *22*, 5592.
- [37] M. A. Croce, F. Boraldi, D. Quaglino, R. Tiozzo, I. Pasquali-Ronchetti, *Eur. J. Histochem.* **2003**, *47*, 63.
- [38] R. C. Savani, G. Y. Cao, P. M. Pooler, A. Zaman, Z. Zhou, H. M. DeLisser, *J. Biol. Chem.* **2001**, *276*, 36770.
- [39] J. M. Rios de la Rosa, A. Tirella, A. Gennari, I. J. Stratford, N. Tirelli, *Adv. Healthcare Mater.* **2017**, *6*, 1601012.
- [40] C. Forster-Horvath, L. Meszaros, E. Raso, B. Dome, A. Ladanyi, M. Morini, A. Albini, J. Timar, *Microvasc. Res.* **2004**, *68*, 110.
- [41] J. Ringel, R. Jesnowski, C. Schmidt, J. Ringel, H. J. Kohler, J. Rychly, S. K. Batra, M. Lohr, *Teratog., Carcinog., Mutagen.* **2001**, *21*, 97.
- [42] a) L. Vistejnova, B. Safrankova, K. Nesporova, R. Slavkovsky, M. Hermannova, P. Hosek, V. Velebny, L. Kubala, *Cytokine* **2014**, *70*, 97; b) G. M. Campo, A. Avenoso, A. D'Ascola, V. Prestipino, M. Scuruchi, G. Nastasi, A. Calatroni, S. Campo, *Curr. Med. Chem.* **2013**, *20*, 1162.
- [43] G. I. Mun, Y. C. Boo, *Am. J. Physiol.* **2010**, *298*, H2102.
- [44] C. B. Knudson, K. T. Rousche, R. S. Peterson, G. Chow, W. Knudson, in *The Many Faces of Osteoarthritis* (Eds: V. C. Hascall, K. E. Kuettner), Birkhäuser, Basel, Switzerland **2002**, p. 219.
- [45] V. Orian-Rousseau, L. F. Chen, J. P. Sleeman, P. Herrlich, H. Ponta, *Genes Dev.* **2002**, *16*, 3074.
- [46] T. L. Cuellar, D. Barnes, C. Nelson, J. Tanguay, S. F. Yu, X. Wen, S. J. Scales, J. Gesch, D. Davis, A. van Brabant Smith, D. Leake, R. Vandlen, C. W. Siebel, *Nucleic Acids Res.* **2015**, *43*, 1189.
- [47] A. Tirella, K. Kloc-Muniak, L. Good, J. Ridden, M. Ashford, S. Puri, N. Tirelli, *Int. J. Pharm.* **2019**, *561*, 114.